Mechanical and fracture behavior of a fiber-reinforced bioabsorbable material for orthopaedic applications

J. L. CHARVET
Department of Mechanical Engineering, Stevens Institute of Technology, Hoboken, NJ 07030
E-mail: jcharvet@yahoo.com

J. A. CORDES
Department of Mechanical Engineering, Stevens Institute of Technology, Hoboken, NJ 07030
E-mail: jcordes@stevens-tech.edu

H. ALEXANDER
Orthogen Corporation, 530 Morris Avenue, Suite 204, Springfield, NJ 07078
E-mail: halexander@aol.com

Tensile and fracture tests were conducted on thin panels of a fiber-reinforced bioabsorbable material. The composites were made of polycarbonate matrix and calcium phosphate fibers. Both matrix and fibers were bioabsorbable orthopaedic biomaterials. The fibers were short and randomly distributed. The properties were compared for composites with and without a coating of methane on the fibers. Composites with the methane coating had a higher elastic modulus, a higher proportional limit, but a lower load at failure on pre-cracked panels. Electron microscopy showed that the coating resulted in a better bond between the matrix and the fiber.

Introduction

A variety of mechanical devices are used to fix broken bones. These devices include staples, screws, plates, and pins. The selection of a device depends on the patient's age, the affected bone, the existence of multiple traumas, the severity of the injury, personal preference and the clinical experience of the surgeon [1]. Most bone implants are made up of metals such as titanium, cobalt-chromium, and stainless steel. These metals are often removed after healing has occurred to prevent atrophy of the bone.

If bioabsorbable materials are used to fix broken bones, second surgeries may not be required [2–5]. When inside the body, the strength and stiffness of these materials decreases over time. This is a desirable. As the bone repairs itself, the load gradually transfers from the mechanical device to the bone. Instead of atrophy, degradable polymers lead to strong replacement bones.

Most absorbable materials are synthetic polymers that contain an ester group. These ester groups degrade in water. The synthetic polymers are derived from one of the following: polylactic acid [6–7], polyglycolic acid [6–7], polydioxanone [8], desamino-tyrosine derived polycarbonates [8–10], polyhydroxy acids, polyphosphoester, or polyanhydride. The polymers alone lack strength and stiffness for load-bearing applications. The stiffness of bioabsorbable polymers ranges from 1–10 GPa. The stiffness of bone is around 20 GPa [12].

Polymers with absorbable reinforcement fibers have been fabricated [13]. These composites have higher strength and stiffness than the polymer alone. The fibers include synthetic forms of hydroxyapatite, the mineral responsible for the high stiffness in bone. Example fibers include synthetic hydroxyapatite crystals, calcium phosphate (glass) fibers [14–15], and calcium sulphate ($CaSO_4$) crystals. The synthetics are stiff and their degradation products bind to bone.

A previous study was conducted on a composite with a polycarbonate matrix and CaP glass fibers [16]. The fibers doubled the stiffness of the polycarbonate. The strength and stiffness was compared for composites with and without a surface modification of the fibers. The previous study did not evaluate the fracture resistance of the composite, an important consideration in the design of orthopaedic devices. This study repeats the fabrication process, the strength tests, and the stiffness tests. This study also compares the fracture resistance of pre-cracked panels with and without surface modification of the fibers.

Materials and methods

Materials

Poly(DTE carbonate) was used as the matrix material for the composite. It had a starting molecular weight of 80,000 Da. The polymer appeared fibrous and white. The

Chemistry Department of Rutgers University supplied the polymer. The fabrication process is well established [17]. Calcium phosphate (CaP) glass fibers were used to reinforce the polycarbonate. They had uniform circular cross-sections with a nominal diameter of 18 μm. The fibers were based on a CaO-P_2O_5-Fe_2O_3 glass system developed at Alfred University [14]. The properties of the matrix and fibers are summarized in Table I.

Fiber surface modification

To improve the bond between the fiber and matrix, CaP fibers were plasma coated with methane (CH_4). The technology included a reactor chamber, a frequency generator, a gas valve and vacuum pump, and a control system [18]. The thickness and surface energy of the coating was proportional to the exposure time. For this process, a 10-minute exposure yielded a 10^3 coat. The fibers were vacuum packed and kept in vacuum until further use.

Fabrication of random, short fiber composites

The fiber composites were fabricated via the wet method, i.e. the prepreg method. All composites produced had 30% fiber by volume. CaP fibers were cut to their optimal packing lengths of 2–3 mm using an electronic cutting device. They were arranged neatly and randomly into a 40×40-mm aluminium foil cavity. The polycarbonate was dissolved in methylene chloride and poured into the cavity containing the fibers. The prepreg was allowed to dry 24 h in a vacuum prior to heat processing.

The prepregs were compression molded using a Carver Laboratory Press Model C with top and bottom-heated platens and water heat exchangers. The stainless steel mold used was frame-type, with a cavity measuring $40 \times 40 \times 0.67$ mm. A thermocouple was used to measure the temperature of the mold. Because the polymer sticks on the mold surface, Teflon sheets (0.01-mm thick) were used to ease the removal and prevent damage of the processed composite. The prepregs were cut into four equal sizes, stacked, and placed in the center of the mold for better fiber distribution. The mold was closed without pressure and was introduced to the heated platens. The composite was processed at 120 °C and 20.3 MPa for five minutes and was allowed to cool at a rate of 30 °C/min. After processing the composite was removed and stored in vacuum.

Sample preparation

Specimens were based on ASTM D3039-76 [19] with slight modification in size due to high material cost. Composite sheets were cut into strips of 40×5.2 mm using a heated knife. The sides were machine polished with a 600-grit carborundum paper to approximately

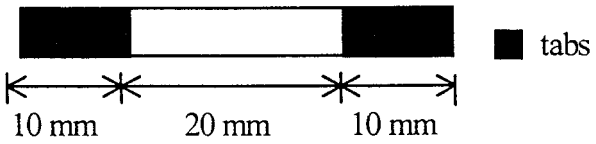

Figure 1 Fracture specimen. Nominal dimensions: $40.0 \times 5.0 \times 0.67$ mm. The cross-sectional area is 3.35 mm^2. Tensile tests did not have a pre-crack.

5.0 mm. Tabs that were made of cellulose triacetate were glued to the ends of the panels. As shown in Fig. 1, the tabs were positioned so that the gauge length of the sample was 20 mm. All samples used were free of cracks and notches in its outer surface. For composites with and without fiber coating, ten specimens without cracks were used for tensile testing.

Pre-cracked panels had crack lengths corresponding to 0.10 W, 0.15 W and 0.25 W, where W is the panel width. There were 10 samples for each crack length. The mean width and thickness of each sample were obtained from three different measurements along the length of the samples. Sample and crack dimensions were measured using a TCL-Image digitizing system interfaced to a light microscope. Notch fabrication was consistent with ASTM E338-81 [20] on sharp notch testing. Cracks were made using a heated probe under a light microscope ($25 \times$).

Tensile tests on thin panels

Tensile tests were conducted on specimens without a center pre-crack. The testing conditions were based on ASTM D3039-76 [19] and were carried out using the Instron Uniaxial Testing Apparatus Model 1321 with pneumatic grips. A 10 kN load cell was used to measure the load. All samples were pulled at a constant crosshead speed of 0.2 mm/min until failure. Load/displacement curves were obtained using the LabTech software program. Data points and specimen dimensions were transferred to a spreadsheet for conversion to stress versus strain points. The elastic modulus of each control specimen was calculated using the first 25 points by linear regression. For each material, the elastic moduli were determined from ten specimens. Other mechanical properties from the tensile tests were based on an average of five specimens. Student's unpaired *t*-test was used to assess the statistical difference between the two materials as well as between the same material with various crack lengths.

Electron microscopy

The fracture surfaces were observed under the scanning electron microscope. Five specimens from each crack size were randomly chosen. The samples were fixed with

TABLE I Properties of the matrix and the fibers

Property	Poly(DTE carbonate)	CaP glass fibers
Elastic modulus, E (GPa)	1.70	50.00
Density, ρ (g/cm^3)	1.20	2.86
Glass transition temperature, T_g (°C)	96	570

epoxy on a specimen dish and were allowed to dry. The samples were sputter-coated using a Denton Vacuum Sputter System (Desk 1 Model). The coated specimens were examined under a scanning electron microscope (JEOL model JSM-T300).

Results

Tensile tests

The stress versus strain diagrams for the composites with and without surface modification of the fibers are shown in Figs 2 and 3. Ten tests were conducted for each material type. The mechanical properties of the composites are summarized in Table II. Improvements to the elastic modulus, elastic limit strength, and yield strength were observed when the fiber surface was modified. The elastic modulus for both the modified and unmodified fiber composites were similar to what was found earlier [16]. In this study, the difference in their stiffness was statistically very significant. The p-value corresponding to the Student's t-test was $p < 0.005$. The chemical coat on the surface modified fibers increased the overall stiffness of the composite by almost 20%.

The proportional limit strength and the yield strength were estimated from the true stress/strain points. The engineering stress versus strain data, σ_{nom} versus ε_{nom}, was converted to true stress versus true plastic strain using the following equations:

$$\sigma_{true} = \sigma_{nom}(1 + \varepsilon_{nom}) \quad (1)$$

$$\varepsilon_{ln}^{pl} = \ln(1 + \varepsilon_{nom}) - \frac{\sigma_{true}}{E} \quad (2)$$

where E is the Young's modulus. For stresses less than the assumed proportional limit strength, the associated ε_{ln}^{pl} was negative. The yield strengths were determined at $\varepsilon_{ln}^{pl} = 0.002$ true plastic strain. The second order curve-fit equation was used to define the nonlinear properties.

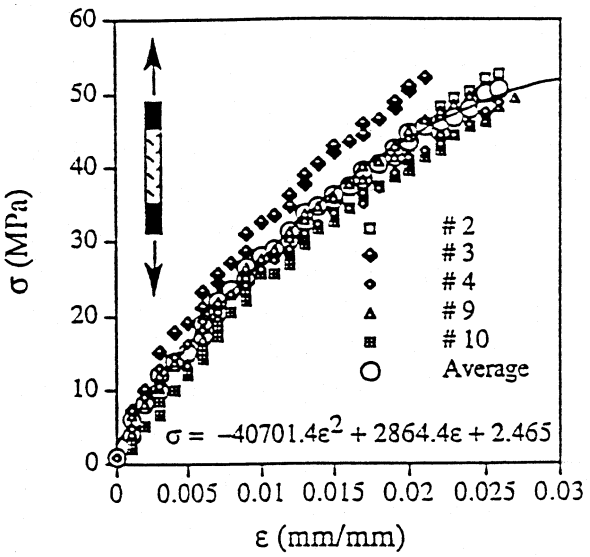

Figure 2 Tensile stress-strain curves of unmodified fiber composite specimens. The second order curve-fit equation was used to define the nonlinear properties of the material.

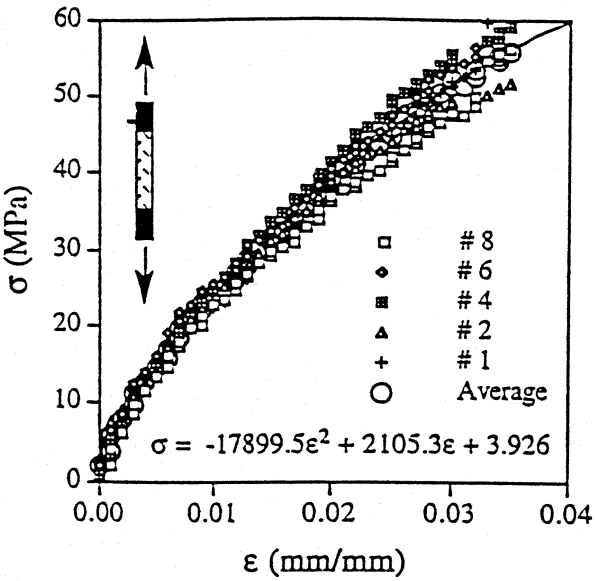

Figure 3 Tensile stress-strain curves of modified fiber composite specimens.

Fracture tests

The stress-strain curves for cracked specimens are shown in Figs 4 (a, b, c) and 5 (a, b, c). All samples had damage prior to fracture. There was a wide variation in the failure loads. The loads at failure for different crack lengths are summarized in Table III. All specimens failed by unstable crack growth. In this study, the composite with fiber surface modification failed at lower loads when the crack length was 0.10 W and 0.15 W. When the crack was large, there was little difference in the failure load between the two materials.

TABLE II Mechanical properties of composites

Type of fiber	Elastic modulus (MPa)	Proportional limit strength (MPa)	Yield strength (MPa)	Failure strength (MPa)	Failure strain (mm/mm)
Unmodified	2290 ± 173	25.00	37.71	56.78 ± 6.65	3.42 ± 0.79
Modified	2850 ± 187	43.00	48.25	50.12 ± 5.40	2.73 ± 0.61

TABLE III Applied load at failure (MPa)

Type of fiber	0.10 W	Crack length 0.15 W	0.25 W
Unmodified	52.6 ± 4.70	47.8 ± 4.52	40.8 ± 4.75
Modified	47.1 ± 2.58	43.6 ± 5.49	40.4 ± 4.08

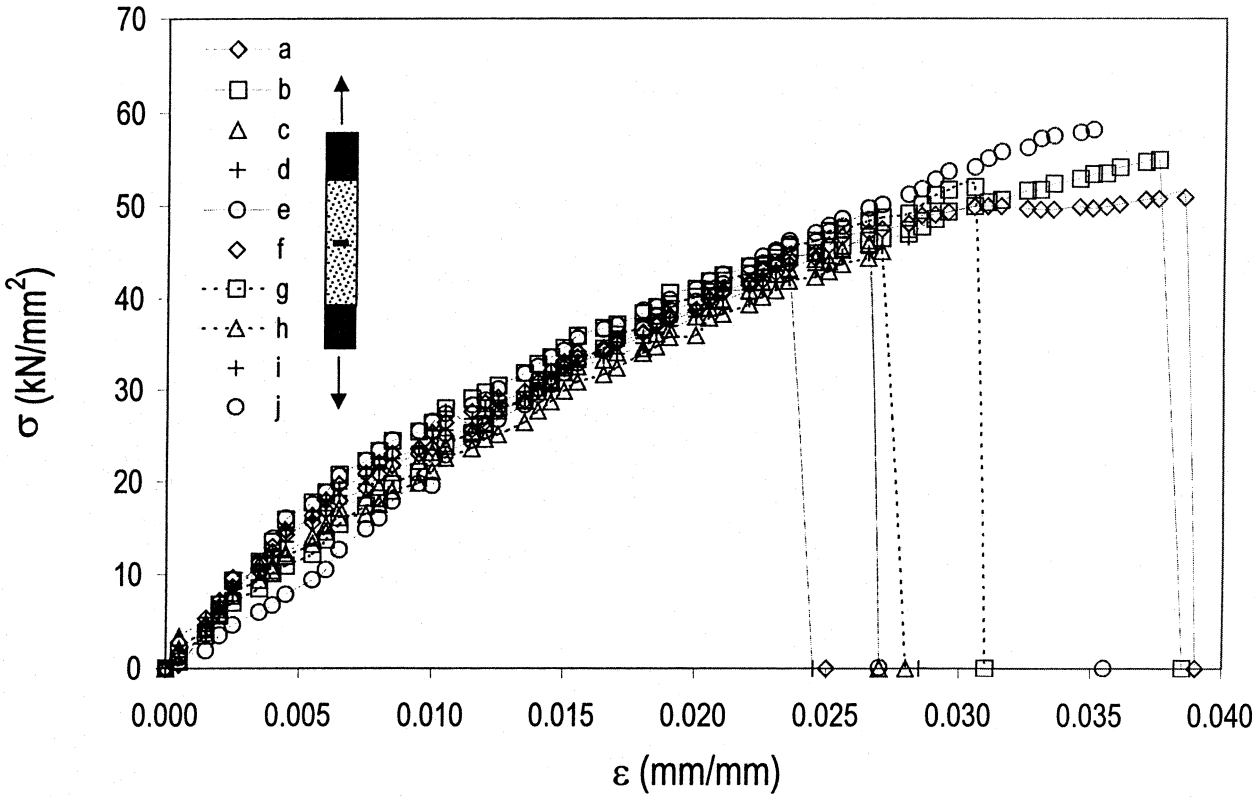

Figure 4a. Stress-strain curves of unmodified fiber composite specimens with $\lambda = 0.10$ crack lengths

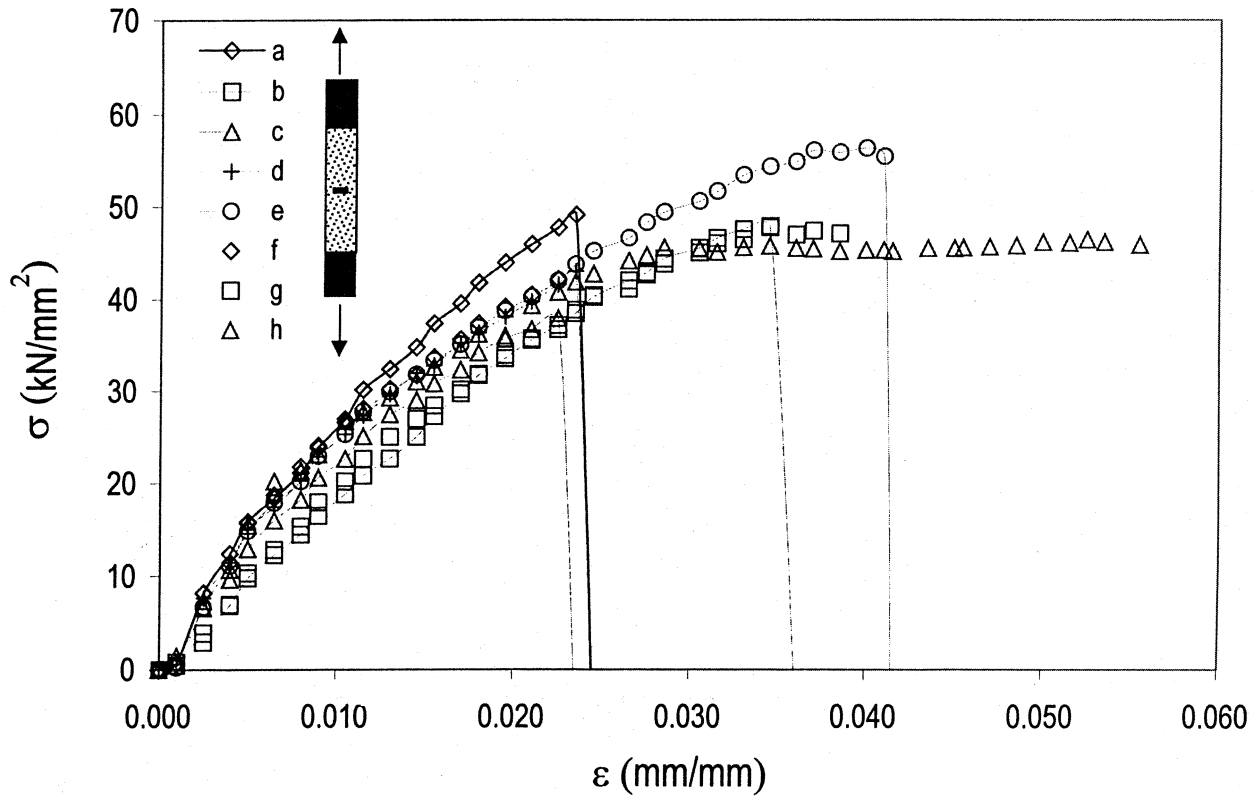

Figure 4b. Stress-strain curves of unmodified fiber composite specimens with $\lambda = 0.15$ crack lengths

Electron microscopy

The fracture sites of the specimens were viewed under a scanning electron microscope. The direction of unstable crack growth was the same as the original crack direction. However, the local mode of fracture appeared to depend on the local orientation of the fibers and the length of the pre-crack.

Fiber pullout was evident in all samples, as shown in Fig. 6. By observation, the number of fiber pullout appeared to depend on the crack length. Specimens with longer cracks exhibited a larger number of fiber pullout. In rare cases, fiber fracture was found. However, this was always accompanied by a pullout of that fiber.

Group (or fiber bundle) pullout was also found in some

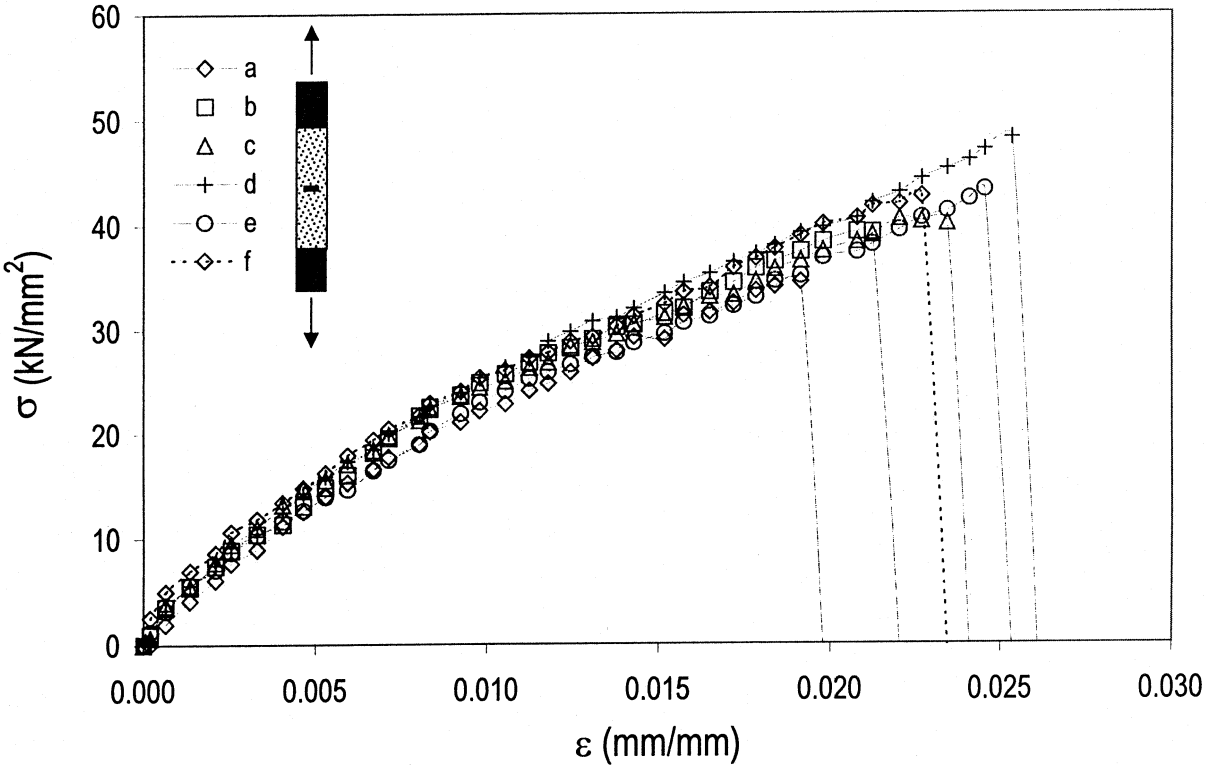

Figure 4c. Stress-strain curves of unmodified fiber composite specimens with $\lambda = 0.25W$ crack lengths

samples, Fig. 7, but it did not depend on the crack length. A cluster of fibers and matrix at the fracture site characterizes group pullout. For this case, the fibers were usually aligned to the direction of the loading. Similar behavior was observed in another study using unidirectional long-fiber composites [21].

For both materials, the orientation of the fibers at the crack tip determined the local crack direction. The average specimen width was 5.0 mm. Fibers were 2–3 mm in length. When the local fiber orientation was approximately perpendicular to the original direction of the crack, fibers were pulled-out, and self-similar crack

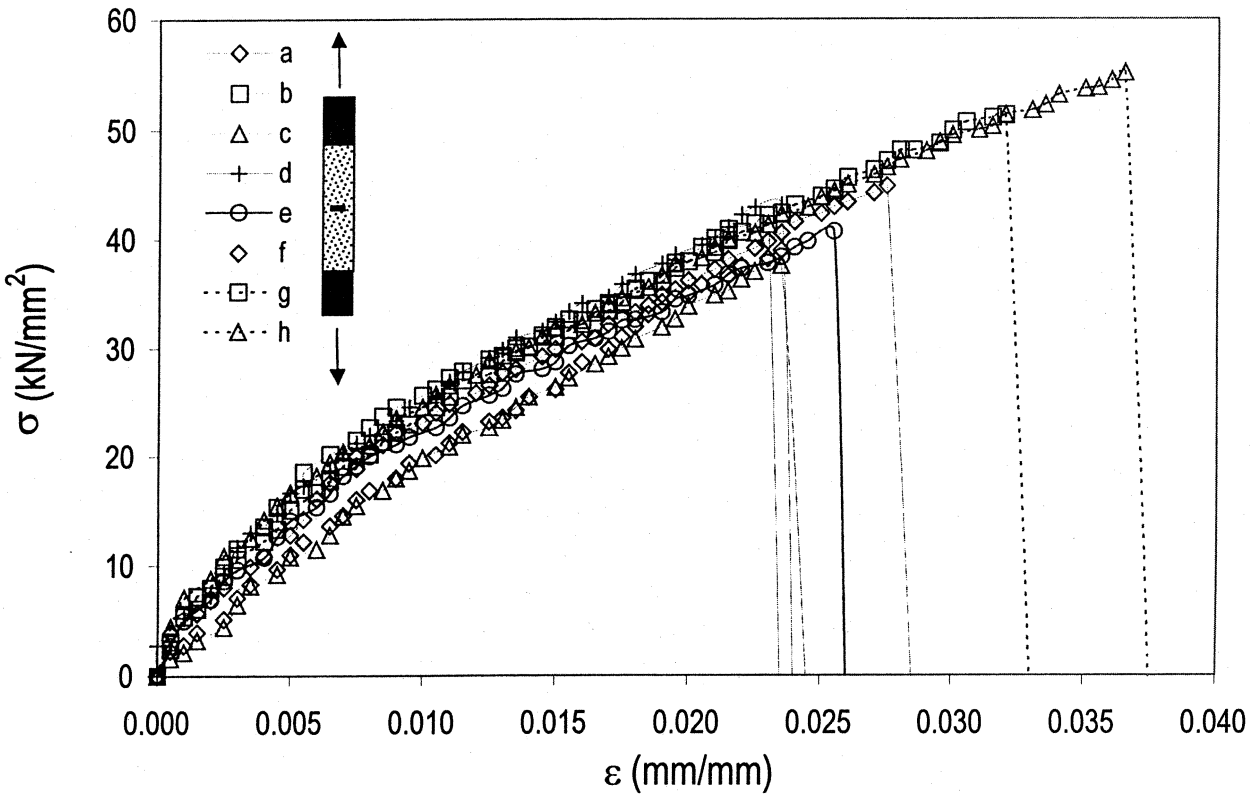

Figure 5a. Stress-strain curves of modified fiber composite specimens with $\lambda = 0.10W$ crack lengths

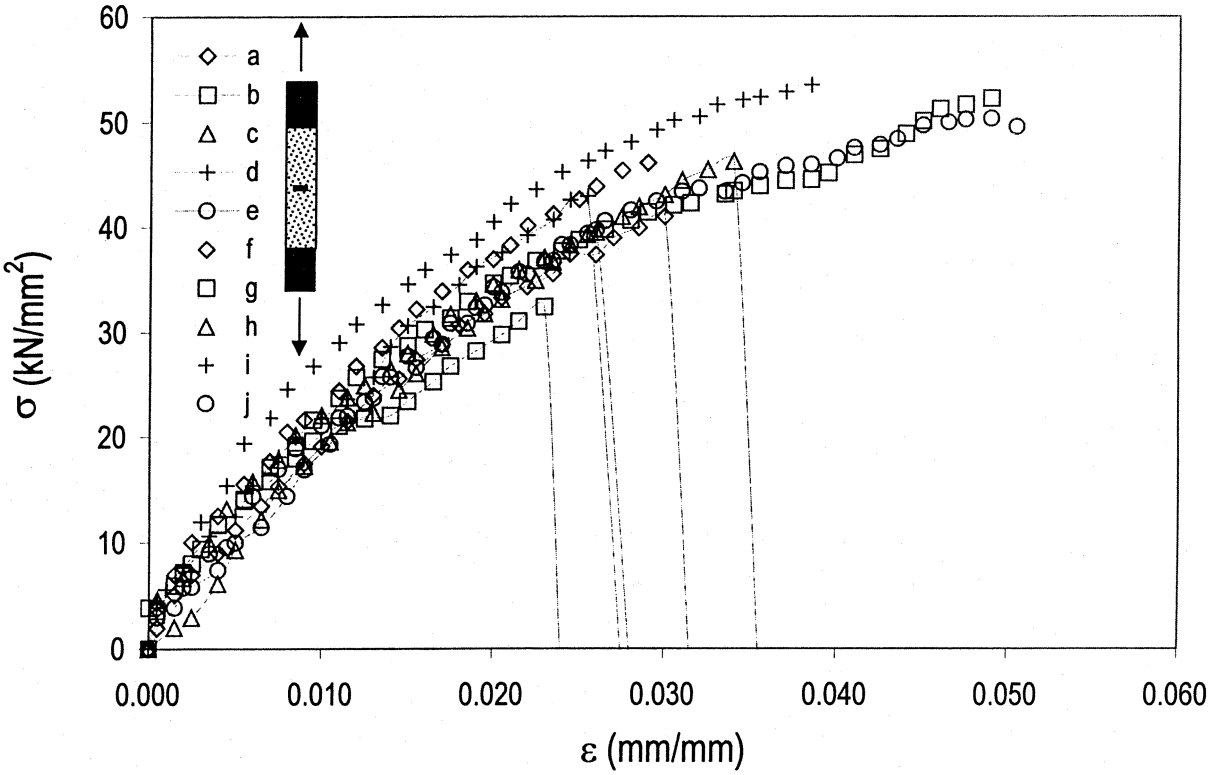

Figure 5b. Stress-strain curves of modified fiber composite specimens with $\lambda = 0.15W$ crack lengths

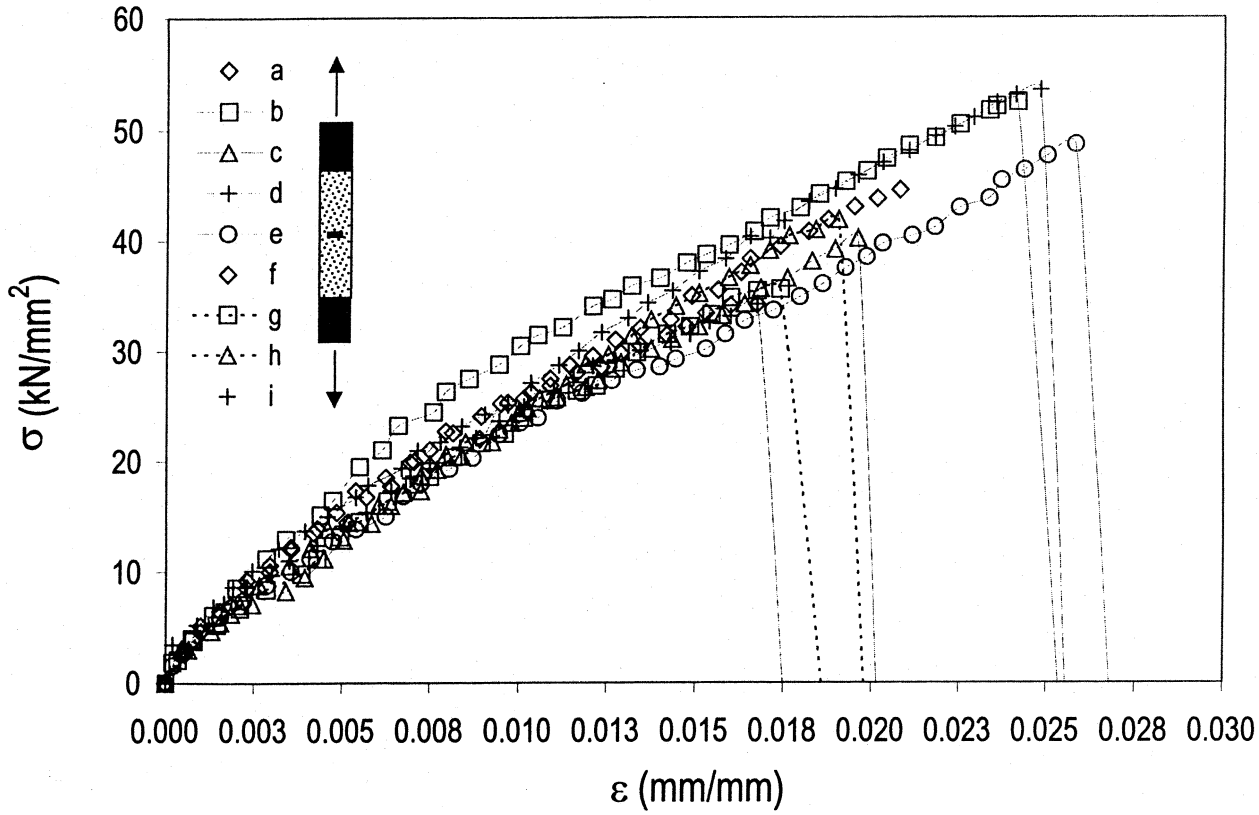

Figure 5c. Stress-strain curves of modified fiber composite specimens with $\lambda = 0.25$ crack lengths

growth occurred along a jagged edge in the direction of the crack length. When the fibers were at relatively high angles with respect to the crack length ($> 45°$), some fiber-matrix debonding occurred, as shown in Fig. 8. This was true for both short cracks and for long cracks as well as for surface modified fibers and unmodified fibers. For this case, the crack propagated along the fiber length. Still, failure of the specimen occurred in a self-similar

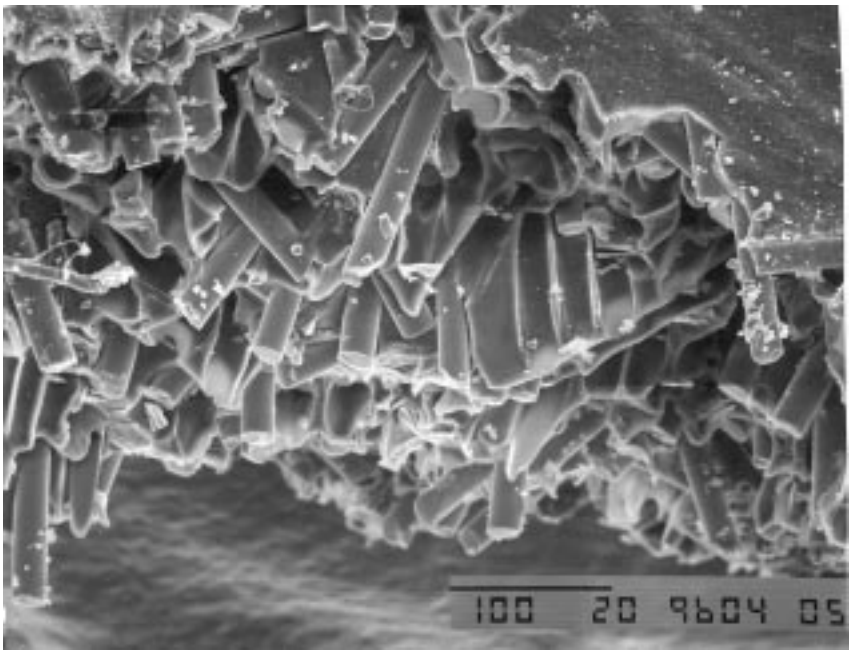

Figure 6 Unmodified fiber composite with a $\lambda = 0.15$ W crack length (200 ×). Protruding fibers and holes at the damage area representing fiber pull-out.

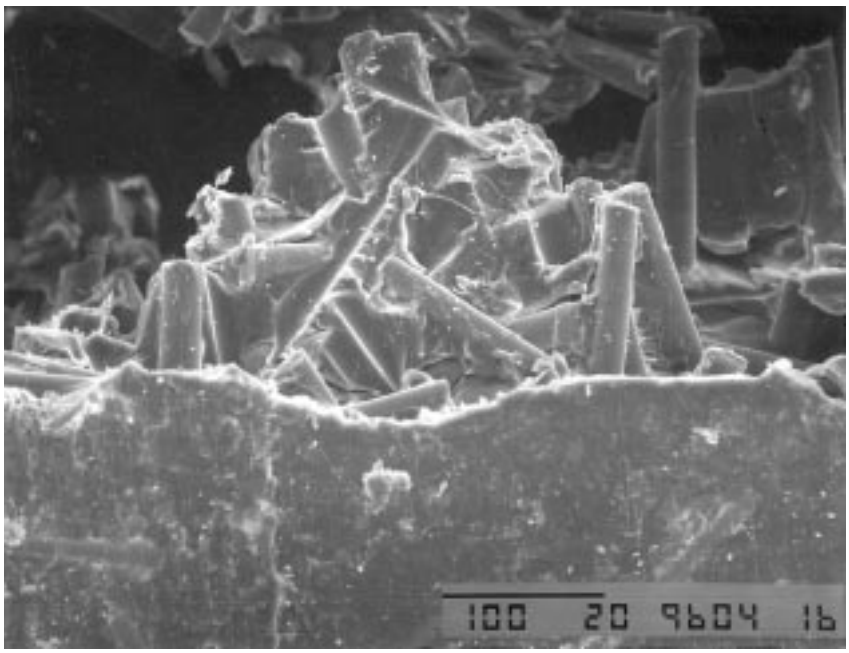

Figure 7 Modified fiber composite with a $\lambda = 0.15$ W crack length (200 ×). When fibers are clumped together, they create a stress concentrated region prone to group fiber pull-out.

fashion, with a jagged surface along the original direction of the crack length.

There was a difference between the fracture behavior between composites without fiber surface modification and those with the surface modifications. With a fiber surface modification, specimens with a crack length of 0.10 W exhibited crack branching, shown in Figs 9 and 10. The location of the multiple fracture site was independent of local fiber orientation of that region and was not associated with the stress concentration near the crack.

There were also instances when the crack did not initiate at the crack tip. In these rare cases, it is postulated that the local stress concentrations are created due to poor fiber distribution.

Conclusions

In this study, short-fiber composites were evaluated experimentally. Plasma coating resulted in an increase in the elastic modulus, yield strength, and proportional limit. This improvement is probably due to the improved matrix/fiber bonding that was noted in the microscopy studies.

Specimen with small cracks probably failed by yield-like behavior. This would account for the relatively large

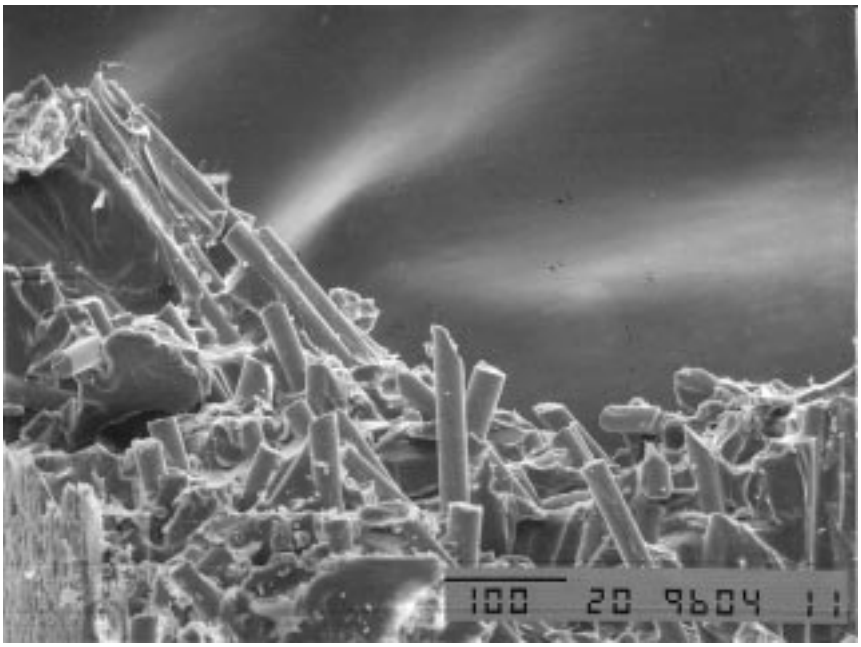

Figure 8 Modified fiber composite with a $\lambda = 0.15$ W crack length (100 ×). The local crack direction is controlled by the fibers. Fibers debonded from the matrix and the crack direction is about 25° from the horizontal.

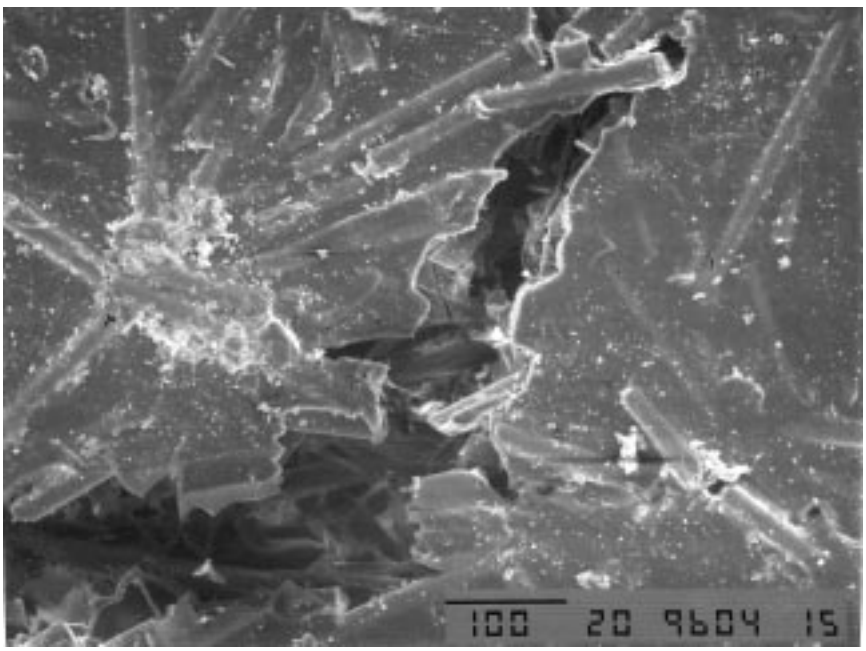

Figure 9 Modified fiber composite with a $\lambda = 0.10$ W crack length (150 ×). Specimens with surface modified fibers and small cracks exhibited multiple fractures at the crack tip.

load line displacement at failure for the two smaller crack lengths. It also explains the difference in load at failure; the stress strain diagram indicates that the material with unmodified fibers can support higher strains.

The use of plasma coating on fibers for composites is an option for the designers of orthopaedic implants. Fiber coatings are recommended for regions where high strength and stiffness are required. However, in regions where large strains are likely, modification of the surface fibers may not provide a superior design. In all cases, the variation of the strength should be considered.

Acknowledgments

The project was aided by funding from Antonio U. Miranda; Integra LifeSciences, Plainsboro, NJ; and the National Institute for Standards and Technology under the grant number 70NANB4H1501. The authors are grateful to Joachim Kohn of Rutgers University for the tyrosine polymer, William La Course of SUNY Alfred for the calcium phosphate fibers, Il Houng Loh of Advanced Surface Technologies for the plasma coating, and John Ricci of the UMDNJ for reviewing this report.

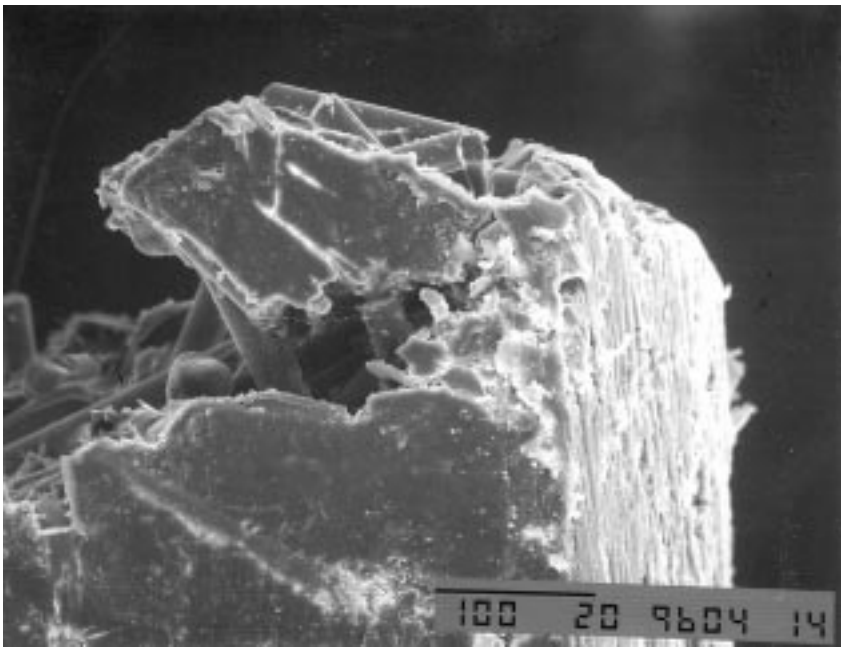

Figure 10 Modified fiber composite with a $\lambda = 0.10$ W crack length (100 ×). Specimens with surface modified fibers and small cracks exhibited multiple fractures away from the crack tip. Here a crack advances to a different direction from the main crack that caused the specimen to fail.

References

1. E. Y. S. CHAO, H. T. ARU and N. INOUE, ''Engineering Principles for Bone Fracture Fixation and Repair,'' in Biomedical Applications of Synthetic Biodegradable Polymers, Edited by J. O. Hollinger (CRC Press, Boca Raton, 1995) p. 145.
2. M. H. MAYER and J. O. HOLLINGER, ''Biodegradable Bone Fixation Devices,'' in Biomedical Applications of Synthetic Biodegradable Polymers, edited by J. O. Hollinger (CRC Press, Boca Raton, 1995) p. 173.
3. C. C. P. M. VERHEYEN, J. R. DE WIJN, C. A. VAN BITTERSWIJK and K. DE GROOT, ''Evaluation of hydroxyapatite-PLLA composite: Mechanical behavior,'' *J. Biomed. Mat. Res.* **26** (1992) 1277.
4. N. R. BOREE, J. DOVE, J. J. COOPER, J. KNOWLED and G. W. HASTINGS, ''Development of a degradable composite for orthopaedic use: mechanical evaluation of an hydroxyapatite-polyhydroxybutyrate composite material,'' *Biomater.* **14** (1993) 793.
5. J. M. ANDERSON, ''Perspectives on the *in vivo* response of biodegradable polymers,'' in Biomedical Applications of Synthetic Biodegradable Polymers edited by J. O. Hollinger (CRC Press, Boca Raton, 1995) p. 223.
6. A. GOPFERICH, ''Mechanisms of polymer degradation and erosion,'' *Biomater.* **17** (1996) 103.
7. K. A. ATHANASIOU, G. C. NIERDERAUER and C. M. AGRAWAL, ''Sterilization, toxicity, biocompatibility and clinical applications of polylactic acid/polyglycolic acid copolymers,'' *Biomater.* **17** (1996) 93.
8. S. I. ERTEL, J. KOHN, M. C. ZIMMERMAN and J. R. PARSONS, ''Evaluation of poly(DTH carbonate), a tyrosine-derived degradable polymer, for orthopaedic applications,'' *J. Biomed. Mater. Res.* **29** (1995) 1337.
9. S. I. ERTEL and J. KOHN, ''Evaluation of a series of tyrosine-derived polycarbonates as degradable biomaterials,'' *J. Biomed. Mat. Res.* **28** (1994) 1.
10. J. CHOUEKA, J. L. CHARVET, K. J. KOVAL, H. ALEXANDER, K. S. JAMES, K. A. HOOPER and J. KOHN, ''Canine bone response to tyrosine-derived polycarbonates and poly(L-lactic acid),'' *J. Biomed. Mater. Res.* **31** (1996) 35.
11. R. A. LATOUR, ''Fiber Reinforced Composite Biomaterials for Orthopedic Implant Applications,'' in Encyclopedic Handbook of Biomaterials and Bioengineering, Part B Vol. 1. D. L. Wise, *et al.* Marcel Dekker, (New York, 1995), p. 359.
12. S. W. SHALABY, ''Bioabsorbable polymers update: degradation mechanisms, safety and applications,'' *J. Appl. Biomat.* **6** (1995) 219.
13. R. F. STOREY and J. S. WIGGINS, ''Design and fabrication of polyester-fibre and matrix composites for totally bioabsorbable biomaterials,'' *Med. Plast. Biomat.* **3** (1996) 41.
14. S. T. LIN, S. L. KREBS, S. KADIYALA, K. W. LEONG, W. C. LACOURSE, B. KUMAR, ''Development of bioabsorbable glass fibres,'' *Biomater.* **15** (1994) 1057.
15. J. CHOUEKA, J. L. CHARVET, H. ALEXANDER, Y. H. OH, G. JOSEPH, N. C. BLUMENTHAL, W. C. LACOURSE, ''Effect of annealing temperature on the degradation of reinforcing fibres for absorbable implants,'' *J. Biomed. Mat. Res.* **29** (1995) 1309.
16. B. J. PEREZ, H. ALEXANDER, C. W. MAYOTT, L. ANDERSON, J. L. CHARVET, J. KOHN, W. C. LACOURSE, I. LOH, ''Effect of fibre-matrix coupling on the mechanical properties of a totally bioabsorbable composite,'' *Trans. of the 5th World Biomater. Congress*, 1996.
17. S. PULAPURA and J. KOHN, ''Trends in the development of bioresorbable polymers for medical applications,'' *J. Appl. Biomat.* **6** (1992) 216.
18. M. S. SHEU, D. M. HUDSON, I. H. LOH, ''Biomaterials Surface Modification Using Plasma Gas Discharge Process,'' in: Encyclopedic Handbook of Biomaterials and Bioengineering, Part A Vol. 1, edited by Wise D. L., *et al.* Marcel Dekker, (New York, 1995) pp. 865–894.
19. ASTM D3039–76, 1995.
20. ASTM E399–81, 1995.
21. J. A. CORDES and R. YAZICI, ''Predicting Crack Growth in Continuous-Fiber Composite Materials,'' in Fracture Mechanics: 26th Vol, ASTM STP 1256. Edited by W. G. Reuter, J. H. Underwood, J. C. Newman (ASTM, Philadelphia, 1995).

Received 30 March 1998
and accepted 29 April 1999